Journal of Biomedical Optics

SPIEDigitalLibrary.org/jbo

Use of multiphoton tomography and fluorescence lifetime imaging to investigate skin pigmentation *in vivo*

Yuri Dancik
Amandine Favre
Chong Jin Loy
Andrei V. Zvyagin
Michael S. Roberts

Use of multiphoton tomography and fluorescence lifetime imaging to investigate skin pigmentation *in vivo*

Yuri Dancik,[a,b*] Amandine Favre,[a] Chong Jin Loy,[c] Andrei V. Zvyagin,[d] and Michael S. Roberts[a,b]
[a]University of Queensland, School of Medicine, Brisbane, Queensland 4102, Australia
[b]University of South Australia, School of Pharmacy and Biomedical Sciences, Adelaide, South Australia 5000, Australia
[c]Johnson & Johnson Asia Pacific, Singapore Research Center, Singapore 038985, Singapore
[d]Macquarie University, MQ Biofocus Research Centre, Sydney, New South Wales 2109, Australia

Abstract. There is a growing body of literature showing the usefulness of multiphoton tomography (MPT) and fluorescence lifetime imaging for *in situ* characterization of skin constituents and the ensuing development of noninvasive diagnostic tools against skin diseases. Melanin and pigmentation-associated skin cancers constitute some of the major applications. We show that MPT and fluorescence lifetime imaging can be used to measure changes in cutaneous melanin concentration and that these can be related to the visible skin color. Melanin in the skin of African, Indian, Caucasian, and Asian volunteers is detected on the basis of its emission wavelength and fluorescence lifetimes in solution and in a melanocyte-keratinocyte cell culture. Fluorescence intensity is used to characterize the melanin content and distribution as a function of skin type and depth into the skin (stratum granulosum and stratum basale). The measured fluorescence intensities in given skin types agree with melanin amounts reported by others using biopsies. Our results suggest that spatial distribution of melanin in skin can be studied using MPT and fluorescence lifetime imaging, but further studies are needed to ascertain that the method can resolve melanin amount in smaller depth intervals. [DOI: 10.1117/1.JBO.18.2.026022]

Keywords: biophotonics; fluorescence; multiphoton processes; tissues.

Paper 12450RR received Jul. 14, 2012; revised manuscript received Dec. 20, 2012; accepted for publication Jan. 29, 2013; published online Feb. 14, 2013; corrected Feb. 20, 2013.

1 Introduction

There is an interest in understanding the relationship between visible skin color and melanin distribution in the skin. Such knowledge could shed further light on the mechanisms regulating skin pigmentation and guide the development of therapies against pigmentation-related pathologies and cosmetic products. In addition, it could provide a deeper understanding of the relationship between the epidermal barrier function and skin pigmentation.[1,2]

The nature and distribution of melanin in the epidermis plays an important role in determining human skin color. After being synthesized in melanocytes, melanin is transferred into neighboring keratinocytes as membrane-bound vesicles termed melanosomes. Melanosomes within the keratinocytes of dark skin individuals tend to be larger and distributed individually, those in light skin Caucasians are smaller and observed as clusters, and in Asian skin they are distributed as a combination of individual and clustered melanosomes.[3]

Current methods to assess the distribution patterns, size, and quantity of melanosomes in the epidermal cell layers are generally invasive, relying on skin biopsies.[3–5] Biopsies are taken from volunteers followed by histological analysis using Fontana-Masson staining, which relies upon the melanin granules to reduce ammoniacal silver nitrate.[6] Alternatively, keratinocyte-melanocyte cocultures are studied using electron ultrastructure microscopy, which relies on the ability to visualize melanin-filled melanosomes by incubation with l-dihydroxyphenylalanine (DOPA).[7] However, these methods fail to precisely define the quantitative profiling of the distribution patterns of melanin due to the inherent physical and chemical limitations of such techniques. For example, despite its simplicity, the nonlinear chemistry of Fontana-Masson staining may yield melanin content measurements that do not correlate with the visual register of skin complexion from different ethnic backgrounds. In addition, electron ultrastructure microscopy involves serial section analysis and three-dimensional reconstruction of the images, which requires instrumentation that may often be inaccessible, and, more importantly, relies on tyrosinase activity that has so far been restricted to melanocytes where melanin is made prior to transfer into epidermal keratinocytes. This suggests that an accurate and quantitative measurement of the quantity and distribution of melanin within the epidermal skin layers may not be attainable with current methodologies. Attempts to use alternative skin color measurements to correlate with epidermal melanin content have also been made but without much impact, including using tristimulus chromameter and photoacoustic methodologies.[8,9]

Multiphoton tomography (MPT) has, in recent years, gained significant traction as a useful method for imaging (highly scattering) biological tissue. Due to the nature of multiphoton absorption and the methods used to implement it, MPT offers significant advantages over single-photon imaging modalities, in particular confocal laser scanning microscopy, for the visualization of biological tissue. Multiphoton imaging is based on the nearly simultaneous [~0.5 fs (Ref. 10)] absorption of generally two or three photons by the fluorophore during near infrared excitation. Since the probability of multiphoton excitation is small, the excitation light must be focused in space and time.[10–12] Spatial focus is achieved using a high numerical

*Present address: The Procter & Gamble Company, Temselaan 100, 1853 Strombeek-Bever, Belgium.

Address all correspondence to: Yuri Dancik, The Procter & Gamble Company, Temselaan 100, 1853 Strombeek-Bever, Belgium. Tel: +32-2-456-6010; Fax: +32-2-568-3750; E-mail: dancik.y@pg.com

0091-3286/2013/$25.00 © 2013 SPIE

aperture (NA) objective. Temporal focus is achieved using a laser which emits ultrashort pulses (10^{-13} to 10^{-14} s) at a high repetition rate.[10–12] The rate of two-photon absorption processes is a function of the square of the light intensity. Photons emitted during two-photon excitation have higher energies than that of the excitation light,[10–12] that is, emission wavelengths are shorter than the excitation wavelengths. The result is high instantaneous, but relatively low average excitation intensity localized within a sub-femtoliter focal volume in the tissue. Fluorophore excitation and emission (fluorescence) occur within this focal volume only precluding out-of-focus excitation,[10–12] which confers the main advantage of multiphoton imaging (tomography) compared with single-photon imaging methods, where the fluorescence signal depends linearly on the excitation intensity. In confocal miscroscopy, a pinhole is used to suppress unwanted out-of-focus fluorescence signal, but its efficiency is limited.[11] Overall, MPT provides higher resolution at greater depths within highly scattering biological tissue in addition to significantly less photodamage.

Fluorescence lifetime is the average time a fluorophore remains in the excited state.[13] Unlike fluorescence intensity, the lifetime depends not on the fluorophore concentration, but on its molecular environment, that is, temperature, pH, viscosity, ionic concentration, oxygen saturation, protein binding, aggregation.[13–15] Fluorescence lifetime imaging (FLIM) provides the ability to discriminate between tissue fluorophores on the basis of their characteristic emission lifetime(s).[13,14]

Optical harmonic generation is another type of nonlinear optical process that takes place in biological tissue under excitation with a femtosecond pulsed laser.[10] Second harmonic generation occurs when two photons coalesce in a scattering process to produce a single photon at exactly twice the photon excitation energy, or half the excitation wavelength.[10,13] This process takes place in materials characterized by an inversion asymmetry and high dielectric permittivity, such as collagenous tissue.

The combination of MPT and FLIM is a useful instrumental hybrid for the investigation of biological tissue *in vivo*. Applications include *in vivo* characterization of tissue components,[16–18] tissue viability,[19] and imaging of dynamic physiological process such as drug distribution and metabolism in liver.[20,21] In addition, MPT and FLIM are emerging as a reliable diagnostic tool for the detection of pigmentation-related skin pathologies.[16,22–28] In skin *in vivo*, MPT yields submicron resolution at a depth of about 200 μm,[29] making the technique well-suited for the detection of lesions occurring in the epidermal basal layer. Table 1 lists the excitation and emission wavelengths, as well as fluorescence lifetimes, of the major skin fluorophores.

A large body of work focuses on the characterization of melanin fluorescence. Tables 2 and 3 summarize published values of melanin fluorescence lifetimes. Beyond the characterization of melanin fluorescence signatures, MPT and FLIM have been used to understand the role of melanin in skin cancers, with *in vivo* imaging performed in healthy skin, nevi, and malignant melanoma.[23–25,49–51] Antoniou et al. have used MPT alone to visualize melanin in different skin types at different depths within the skin.[52] They show qualitatively that fluorescence intensity correlates with melanin concentration. Ait El Madani et al. have demonstrated the utility of MPT and FLIM in characterizing skin depigmentation following the application of a topical corticosteroid.[53]

We have used MPT and FLIM to investigate the relationship between visible skin color and melanin content and distribution in the skin of volunteers. We show here that *in vivo* changes in skin melanin content and distribution, as evidenced by measured

Table 1 Two-photon excitation, emission wavelengths, and fluorescence lifetimes of major endogenous skin fluorophores and collagen second harmonic generation (SHG).

Fluorophore	Investigated systems	Excitation wavelength (nm)	Emission wavelength (nm)	Lifetimes (ps)	References
Elastin	Excised rat and human skin	730 to 830	460 to 575	260, 1960	12, 17, 30, 31
Flavins (FAD)	In solution, excised skin lesions	800 to 900	490 to 650	2300 to 2800 (free) 40 to 400 (bound)	12, 32– 34
Keratin	In solution, human skin biopsies and hair	700 to 900	450 to 550	1400	12, 35, 36
Lipofuscin	Human retinal pigment epithelial cells	800	500 to 550	60, 320, 1200, 4800	12, 37
Melanin	Human retinal epithelial cells, eye fundus, biopsied human skin lesions, hair	750 to 820	550	~100 to 200, ~500 to 1800	See Table 3
NAD(P)H	Cell cultures, *in vivo* hamster pouch cheek epithelial cells, synthetic skin	730 to 800	450 to 480	300 to 700 (free) 2500 to 3000 (bound)	12, 38, 39–41
Porphyrins	*In vivo* chicken embryo membrane, *in vivo* skin lesions	800	590 to 635	5200, 18,000 to 20,000	42–44
Retinol	Ethanol solution, binding to β-lactoglobulin	700 to 830 (free)	~500 (free)	1800, 5000 (free) 700, 3600, 12,000 (bound)	45, 46
Vitamin D2, D3	Sodium phosphate solution, ethanol solution	<700	400 to 500	N/A	46, 47
Collagen SHG	*In vivo* mouse skin, excised human skin	730 to 880	1/2 of excitation wavelength	No lifetime	12, 17, 31, 48

Table 2 Reported fluorescence lifetimes of melanins in solution and cell culture.

Reference	Compound	Excitation method	Excitation wavelength (nm)	Lifetimes (ps)	Observations
54, 55	Synthetic melanin in DMSO	2P stepwise	800	200 ± 20, 1500 ± 200, 5800 ± 200	Three-exponential decay. Selective excitation of melanin at 800 nm.
56	Sepia melanin in water	1P	335	~60, ~500, ~2000, ~7000	Four-exponential decay, lifetimes values are essentially independent of emission wavelength.
57	Sepia eumelanin in water	1P	400	First set: 144, 960, 5030, 11,800 Second set: 121, 800, 5370, 12,800	First set of lifetimes corresponds to large size fractions (MW > 10,000), the second to smaller ones (MW < 1000). Data suggests both size fractions contain different distributions of the same aggregation states.
32	Synthetic eumelanin in water	1P	370	500 to 1000, 2000 to 4000, 7500 to 10,000	Three-exponential decay. Slow τ depends on emission wavelength.
58	DOPA-melanin	2P	750	1200	Similar to black hair containing eumelanin.
59	Sepia eumelanin	2P	775	0.450 ± 0.05, 3 ± 0.5	Short signal is within, large signal is outside the pump pulse overlap.
60	Human melanocyte culture	2P	760 800	151, 1244 106, 1499	Various fluorescence intensities within cells may reflect different melanin contents.

changes in fluorescence intensity arising from constitutive skin pigmentation, can be tracked and interpreted using MPT and FLIM.

2 Materials and Methods

2.1 *Melanin Solution Preparation*

Melanin solutions were prepared by dissolving the melanin (M8631, Sigma-Aldrich) in tris(hydroxymethyl)aminomethane hydrochloride (TrisHCl) and adjusting the pH to 8.0. The solutions were further mixed in an orbital shaker for 8 h. Aliquots of 1 mL were centrifuged at 13,000 rpm for 1 min prior to imaging.

2.2 *Cell Culture*

Human melanoma cells MNT1 and HaCaT keratinocytes were maintained in a 5% CO_2 humidified incubator at 37°C in cell culture medium composed of RPMI 1640 medium (Sigma) supplemented with 10% heat-inactivated fetal calf serum (Sigma) and penicillin-streptomycin (1.25 mL; Sigma). The cells were collected by centrifugation and transferred in a flask containing 10 mL medium. The cells were harvested by treatment with 0.25% Trypsin/EDTA and collected after centrifugation (700 rpm, 3 min) in cell culture medium. The cells were seeded in an OptiCell (Nunc) at a density of 6×10^5 cells/mL and MPT and FLIM imaging was performed 24 h postseeding.

2.3 *In Vivo Skin Color Measurements*

All studies involving volunteers were undertaken with approval from the Princess Alexandra Hospital/University of Queensland Research Ethics committee and written consent from the volunteers. Two male and three female volunteers, aged 19 to 42, from African, Indian, Caucasian, and Asian backgrounds were recruited. A 1-cm^2 area on the right dorsal (photoexposed) and volar (photoprotected) forearm of each volunteer was selected. A Konica-Minolta CM-2600d reflectance spectrophotometer was used to measure the tristimulus $L*$, $a*$, and $b*$ values at three spots within the selected area. The $L*$ value represents brightness from black ($L* = 0$) to white ($L* = 100$). The $a*$ scale is the green to red scale, with $a* < 0$ indicating green and an increase in $a*$ ($a* > 0$) indicating an increase in redness. Similarly, $b*$ represents blue ($b* < 0$) to yellow ($b* > 0$) (Ref. 63). Each set of $L*$, $a*$, $b*$ values was measured using the 3 mm aperture plate provided with the spectrophotometer upon calibration with a white tile.

2.4 *MPT and Fluorescence Lifetime Imaging*

Multiphoton tomography was performed with a DermaInspect (Jenlab, Jena, Germany) equipped with a tunable (710 to 920 nm) Titanium:Sapphire ultrashort-pulse laser (Mai Tai, Spectra Physics). The laser pulse width and repetition rate were 85 fs and 80 MHz, respectively. A broad bandpass filter (BG39, Schott glass color filter) with a 700-nm cutoff was used to block the excitation laser light. *In vitro* and *in vivo* imaging was performed with a high-NA oil-immersion objective (40×, NA 1.3). The FLIM color map distribution was realized by employing a time-correlate single-photon counting (TCSPC) module with time resolution of 200 ps. Images sized 128×128 pixels were recorded in four different spectral channels: channels 1, 2, 3, 4 corresponding to 350 to 450 nm; 450 to 515 nm; 515 to 620 nm; and 620 to 670 nm spectral bands.

2.4.1 *Synthetic melanin solutions*

Inside a rubber O-ring (diameter ~8.35 mm, height ~1.0 mm) glued onto a glass slide, 50 μL aliquots of melanin solution were

Table 3 Reported fluorescence lifetimes of melanins in human skin, hair, and eye.

Reference	Location	Excitation method	Excitation wavelength (nm)	Lifetimes (ps)	Observations
61	Melanin granules isolated from retinal pigment epithelium	1P	364	220, 700, 2200, 8000	Four-exponential decay. Time-gated spectroscopy shows age-related changes in melanin fluorescence.
62	Eye fundus	1P	446	280, 2400	Fluorescence signals from melanin are expected to be weak compared to other fluorophores.
58	Hair	2P	750 to 820	First set: 200, 1300 Second set: 400, 2200	First set obtained from hair due to eumelanin in black hair. Second set due to pheomelanin in blond hair.
	Nevi	2P	750 to 820	400, 1250	
24	Melanocytes in melanocytic nevi and melanomas	2P	760, 800	140 ± 32 1076 ± 357	Melanocytes were distinguished from keratinocytes on the basis of FLIM data. Selective excitation of melanin with wavelength of 800 nm.
60	Forearm skin (basal cells)	2P	760 800	132, 1762 122, 1496	FLIM may reveal differences in melanin content of sun-protected and sun-exposed skin.
	Hair bulb	2P	760 800	97, 537 97, 476	

placed. A glass cover slip was placed on top of the solution such that it remained in contact with the solution. A drop of immersion oil was placed on top of the cover slip, and the slide was placed on a stage for imaging. Melanin solution samples were excited at 800 nm with an incident laser power of 30 mW.

2.4.2 *Cell cultures*

Cells were imaged in triplicates directly in the OptiCell cell culture chamber. A drop of immersion oil was placed on the surface of the OptiCell. The cells were excited at 740 nm for fluorescence intensity imaging and 800 nm for fluorescence lifetime imaging. The incident laser power was 30 mW.

2.4.3 *Volunteers*

A drop of saline solution was placed on the area of skin to be imaged. A metal attachment containing a glass cover slip with a drop of immersion oil was placed directly on the volunteers' skin. The surface of the stratum corneum was first located using an excitation wavelength of 740 nm, which is optimal for skin autofluorescence. Upon localization of the surface, the excitation wavelength was switched to 800 nm for further imaging. Fluorescence intensity and FLIM measurements were then taken at depths of approximately 30 μm (lower stratum granulosum) and 50 μm (stratum basale) below the surface of the skin, on the dorsal and volar sides of the forearm. The incident laser power was constant at 35 mW in order to avoid tissue damage.[64]

2.5 *Data Analysis*

Fluorescence lifetime data analysis was performed using SPCImage 2.9 (Becker & Hickl). Fluorescence was detected within the emission range of 515 to 620 nm, which includes the peak emission wavelengths of melanin, 550 to 575 nm (Refs. 17 and 54). For the images of melanin in solution and of the cell cultures, the bin number was set to 3; for the *in vivo* images, it was set to 4. This number defines the number of adjacent pixels whose photon decay data is used to obtain a photon decay profile and calculate lifetimes in a given pixel. The bin number n is calculated from

$$\text{binned pixels} = (2n+1) \cdot (2n+1). \tag{1}$$

After setting the bin number, regions of interest (ROI) for FLIM analysis were defined such that skin folds, areas of evident photobleaching, and cells out of the focal plane would be avoided in the calculation of lifetimes. The area of the ROI was calculated after calibration using ImageJ®. The time-dependent photon data were fitted to an exponential function, yielding one or more lifetime distributions τ_i (herein given in ps) and the corresponding weighting coefficient a_i (%) of the overall fluorescence decay signal[13]

$$F(t) = \sum_{i=1}^{n} a_i e^{\frac{-t}{\tau_i}}. \tag{2}$$

3 Results

3.1 *MPT Imaging of Synthetic Melanin Solution*

The photon decay profiles obtained from the synthetic melanin solutions of varying concentration (0.5 to 2.0 mg/mL) displayed bi-exponential photon decay profiles, yielding a fast (τ_1) and slow (τ_2) lifetime. Figure 1(a) shows an example of such a profile. Figure 1(b) to 1(d) shows fluorescence pixel

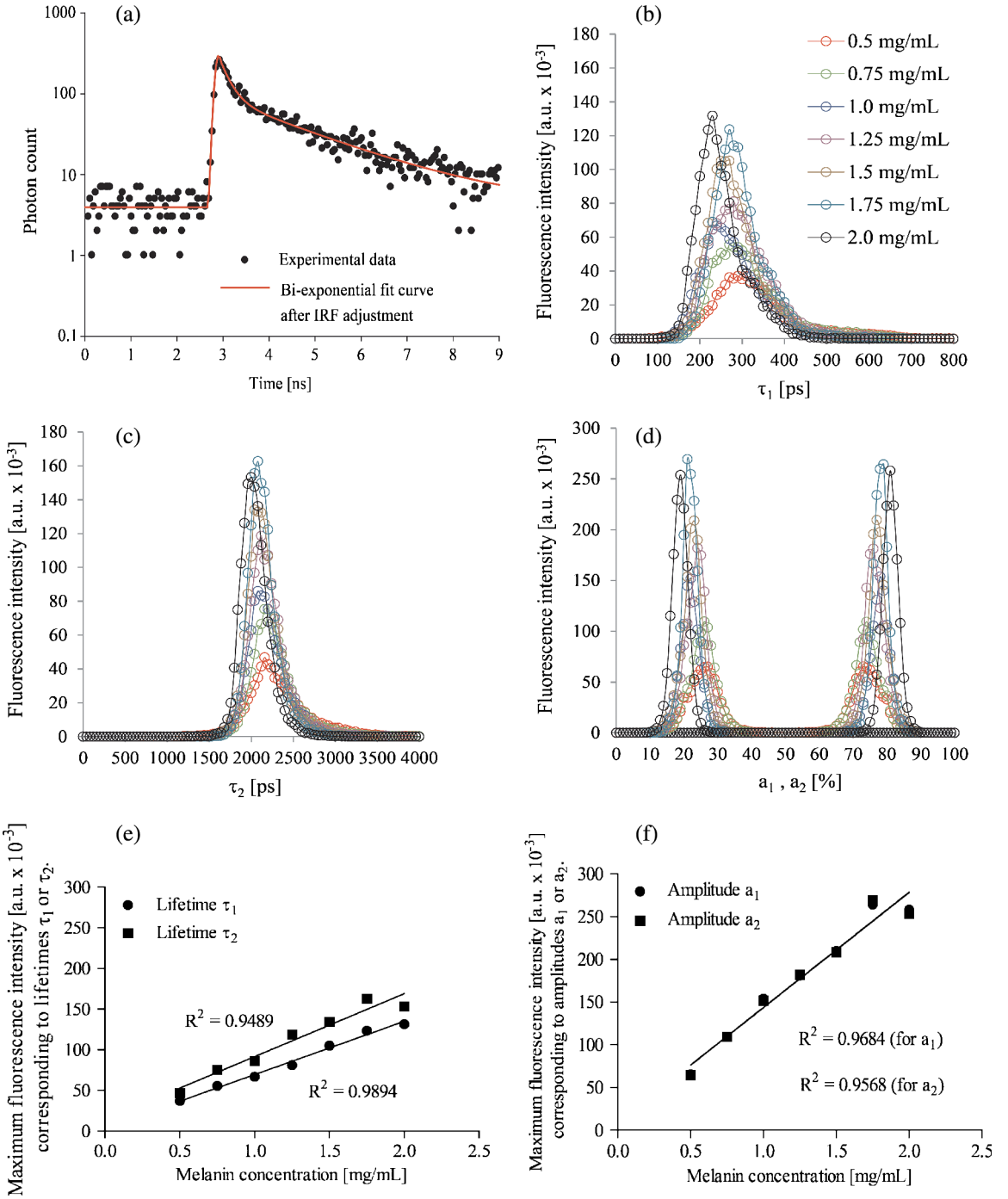

Fig. 1 Fluorescence lifetime imaging data from synthetic melanin in TrisHCl (pH 8): (a) representative photon decay profile from the 1 mg/mL solution. A biexponential curve fits the data, with the reduced coefficient $X^2 = 1.19$. Distribution of (b) the fast lifetime τ_1; (c) the slow lifetime τ_2; (d) the amplitudes a_1 and a_2, at concentrations ranging from 0.5 to 2.0 mg/mL; (e) maximum fluorescence intensity corresponding to τ_1 and τ_2 lifetimes versus melanin concentration; (f) maximum fluorescence intensity corresponding to amplitudes a_1 and a_2 lifetimes versus melanin concentration.

intensity versus lifetime values τ_1 and τ_2, and amplitudes a_1 and a_2. Over the range of concentrations investigated, the lifetimes [mean $\pm$ standard error of the mean $\times$ (s.e.m.)] corresponding to the highest pixel intensity are $\tau_1 = (264 \pm 8)$ ps and $\tau_2 = (2091 \pm 23)$ ps. The corresponding amplitudes (mean $\pm$ s.e.m.) are $a_1 = (77 \pm 0.8)\%$ and $a_2 = (23 \pm 0.8)\%$, indicating that the τ_1 lifetime is the most significant lifetime signature of melanin in solution. Figure 1(e) and 1(f) shows that the maximum pixel intensity associated with lifetime τ_1 increases linearly with melanin concentration from 0.5 to 2.0 mg/mL. The maximum pixel intensity associated with lifetime τ_2 increases linearly for concentrations ranging from 0.5 to 1.75 mg/mL. The correlation coefficient is slightly higher with the τ_1 and a_1 data compared to the τ_2 and a_2 data.

3.2 *Selective Wavelength Imaging of Melanocyte-Keratinocyte Cocultures*

The fluorescence intensity image and FLIM τ_1 color of melanocyte-keratinocyte cocultures excited at 800 nm shows selective

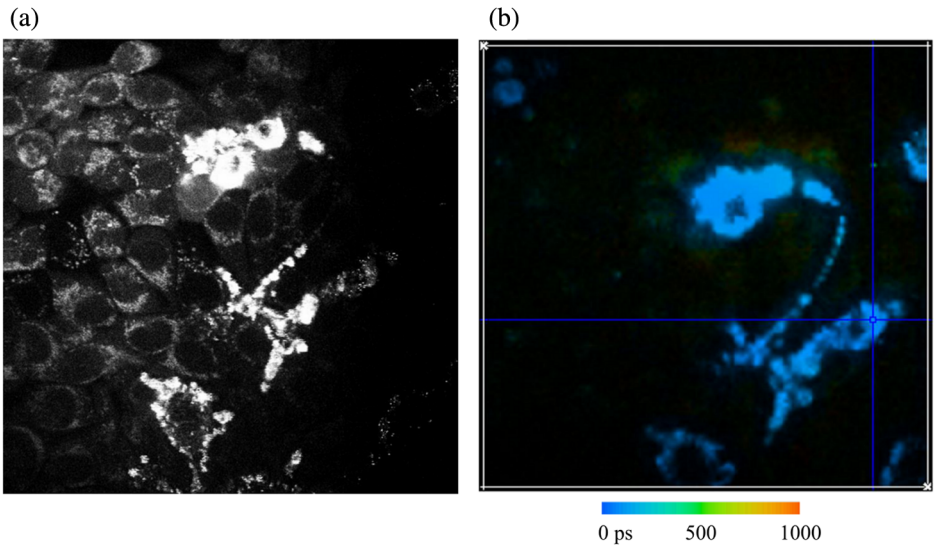

Fig. 2 (a) Fluorescence intensity image and (b) FLIM τ_1 color map of an MNT1 melanocyte-HaCaT keratinocyte coculture obtained upon excitation at 800 nm.

excitation of melanin-producing melanocytes [Fig. 2(a) and 2(b)]. The appearance of strong fluorescence signals within melanocytes corresponds with the melanin granules that extend into the dendrites of melanocytes. FLIM parameters of the melanocyte-keratinocyte cocultures (Fig. 3) show that lifetime values corresponding to the peaks in the melanocyte fluorescence are $\tau_1 \approx 145$ ps [Fig. 3(a)]; $\tau_2 \approx 1883$ ps [Fig. 3(b)]. The amplitude values corresponding to melanin are $a_1 \approx 93\%$, $a_2 \approx 7\%$ [Fig. 3(c)]. A weak fluorescence stemming from the keratinocytes surrounding the melanocytes is seen in Fig. 2(a) and 2(b). The lifetimes associated with the peaks in the keratinocyte fluorescence are $\tau_1 \approx 750$ ps [Fig. 3(a)] and $\tau_2 \approx 3000$ ps [Fig. 3(b)]. This weak fluorescence is likely to be mainly from flavine adenine dinucleotide (FAD), which may be partially excited at 800 nm and has a range of emission wavelengths which overlap with that of melanin (Table 1).

The ability of the imaging system to delineate melanin based on spectral and morphological differences in a biologically mixed environment provides opportunity to observe the distribution of melanin in human skin *in vivo*.

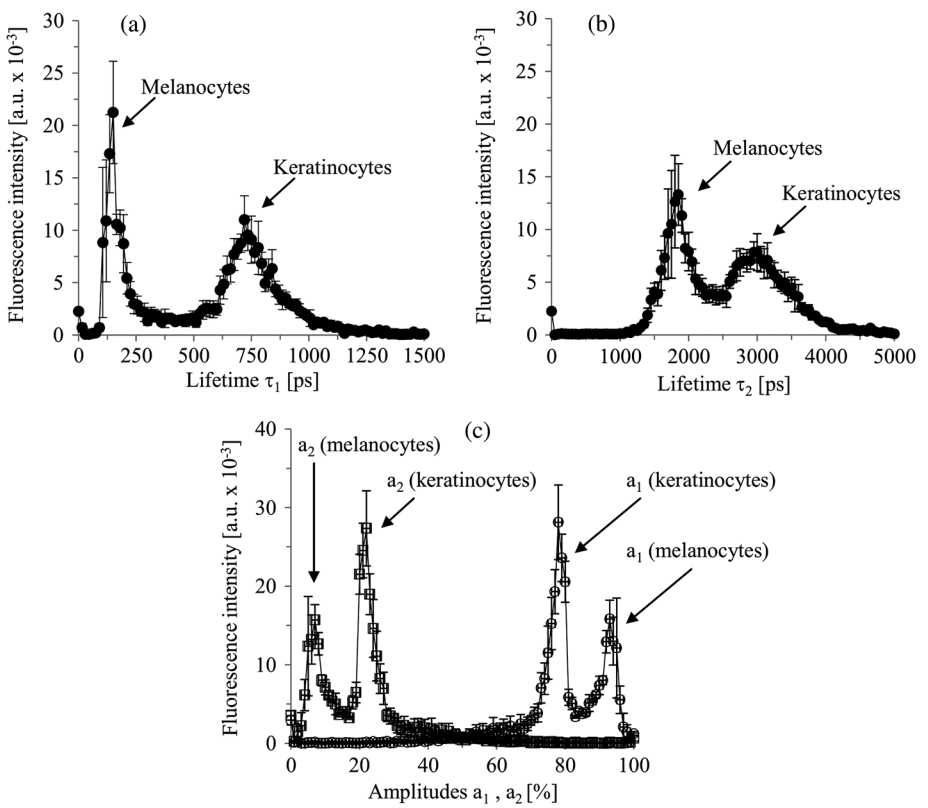

Fig. 3 Fluorescence lifetime distributions obtained from the MNT1 melanocyte–HaCat keratinocytes coculture ($n = 3$ measurements), excitation wavelength 800 nm: (a) fast lifetime τ_1; (b) slow lifetime τ_2; and (c) corresponding amplitudes a_1 and a_2.

Table 4 Mean spectrophotometric data of volunteers (three measurements within a 1 cm^2 area on each side of forearm).

		Dorsal forearm			Volar forearm			
Volunteer	Ethnicity/Gender	$L*$	$a*$	$b*$	$L*$	$a*$	$b*$	$\Delta L*$
1	African/F	31.31	6.99	7.91	33.35	7.50	9.82	2.04
2	Indian/M	46.99	11.33	19.31	52.60	9.20	19.88	5.60
3	Caucasian/F	51.69	9.94	20.97	57.90	7.24	19.13	6.21
4	Caucasian/M	52.16	9.09	20.33	58.52	8.13	17.44	6.35
5	Asian/F	57.42	8.28	17.82	65.63	3.30	14.30	8.20

M = Male, F = Female. $\Delta L* = L*$ (volar) $- L*$ (dorsal).

3.3 *In Vivo MPT Imaging of Epidermal Melanin in Different Healthy Ethnic Skin*

FLIM signatures of differences in human skin melanin content were investigated by comparing dorsal forearm skin of five volunteers of African, Indian, Caucasian, and Asian ethnic backgrounds. Table 4 shows the mean spectrophotometric tristimulus $L*$, $a*$, and $b*$ values acquired from each volunteer forearm. There is a consistent trend where the dorsal side is darker than the volar side, presumably due to increased sun exposure to the former. Interestingly, the contrast ($\Delta L*$) between dorsal and volar skin color is smaller in darker skin compared to lighter skin (Table 4). Figure 4 shows examples of the MPT signal intensity and FLIM color maps from the strata granulosum and basale of the Asian [Fig. 4(a) and 4(b)] and the African [Fig. 4(c) and 4(d)] volunteer. The densely packed keratinocytes of the stratum granusolum layer and the much smaller, polygonal keratinocytes of the stratum basale[12,65] are clearly visible.

The corresponding area-normalized fluorescence intensity versus τ_1 lifetime profiles is shown in Fig. 5. On the dorsal side of the African volunteer's skin, the maximum mean fluorescence intensities are (496 ± 90) a.u./μm^2 at $\tau_1 = 140$ ps and (549 ± 211) a.u./μm^2 at $\tau_1 = 120$ ps in the stratum granulosum and basale, respectively [Fig. 5(a)]. In volar skin, the peak intensities are (440 ± 141) a.u./μm^2 at $\tau_1 = 130$ ps and (521 ± 50) a.u./μm^2 at $\tau_1 = 120$ ps in the stratum granulosum and basale, respectively [Fig. 5(b)]. On the dorsal side of the Asian volunteer's skin, the peak florescence intensity is

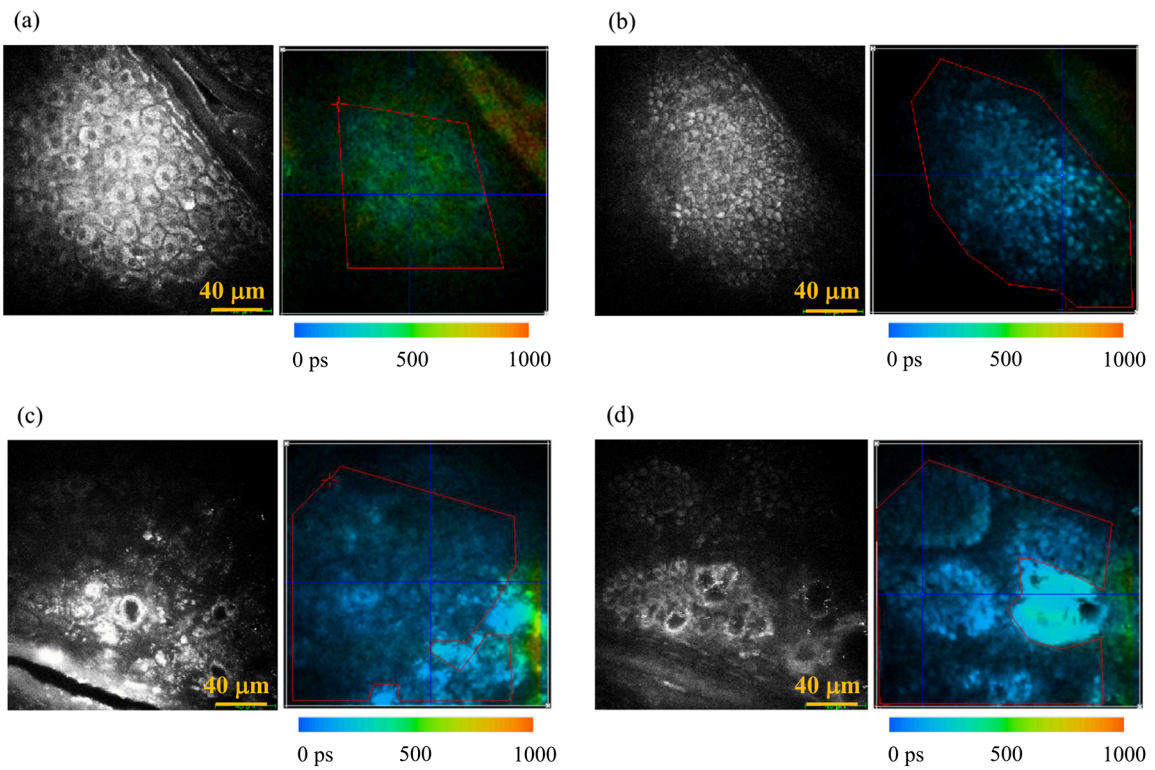

Fig. 4 Fluorescence intensity map after 740 nm excitation and corresponding fast (τ_1) lifetime color maps obtained upon excitation wavelength at 800 nm. Asian volunteer's (a) stratum granulosum and (b) stratum basale. African volunteer's (c) stratum granulosum and (d) stratum basale. The red lines indicate the regions of interest in which the area-normalized fluorescence intensities were calculated.

(203 ± 60) a.u./μm^2 at $\tau_1 = 220$ ps and (195 ± 30) a.u./μm^2 at $\tau_1 = 180$ ps in the stratum granulosum and basale, respectively [Fig. 5(c)]. On the volar side, the peak florescence intensity is (97 ± 44) a.u./μm^2 at $\tau_1 = 280$ ps and (137 ± 106) a.u./μm^2 at $\tau_1 = 150$ ps in the stratum granulosum and basale, respectively [Fig. 5(d)].

Figure 6 shows the mean fluorescence intensity versus τ_2 lifetime profiles obtained from the same FLIM measurements. The profiles obtained from the stratum granulosum of the African volunteer's skin display maximum fluorescence intensities of (148 ± 67) a.u./μm^2 and $((128 \pm 34)$ a.u./μm^2 on the dorsal and volar skin sides, corresponding to τ_2 lifetimes of 1800 and 1720 ps, respectively [Fig. 6(a) and 6(b)]. On the other hand, two distinct peaks in maximum fluorescence intensity are obtained from the stratum basale: (89 ± 45) and (131 ± 33) a.u./μm^2 corresponding to $\tau_2 = 520$ and 1760 ps on the dorsal side and (100 ± 59) and (80 ± 22) a.u./μm^2 corresponding to $\tau_2 = 640$ and 1680 ps on the volar side [Fig. 6(a) and 6(b)]. The skin of the Asian volunteer yields single maxima in mean fluorescence intensities. In the stratum granulosum, these are (242 ± 21) a.u./μm^2 and (138 ± 47) a.u./μm^2, both at $\tau_2 = 1920$ ps, in dorsal and volar skin [Fig. 6(c) and 6(d)]. In the stratum basale, the peak intensities are (203 ± 40) a.u./μm^2 at $\tau_2 = 1840$ ps in dorsal skin and (72 ± 31) a.u./μm^2 at $\tau_2 = 1760$ ps in volar skin.

3.4 *Correlation Between the Fluorescence Intensities and Skin Pigmentation*

Figure 7(a) through 7(d) shows that the mean maximum fluorescence intensities corresponding to the τ_1 lifetime in the stratum granulosum and basale on the dorsal and volar forearm correlates with the measured mean $L*$ value. These data show a general trend in which fluorescence intensities decreases linearly with increasing skin color lightness (increasing mean $L*$ value) when two clusters of skin types are considered: the darkly pigmented African skin and the lighter pigmented skin types (Indian, Caucasian, and Asian skin). The correlation between fluorescence intensities and mean $L*$ values are significantly weaker when only the cluster to lightly pigmented skin types is considered.

Alaluf et al. showed a correlation between total melanin content and $b*$ for lightly pigmented skin types.[63] Removing the data points obtained from African skin, we obtain significant correlations between the maximum fluorescence intensities in the dorsal and volar stratum granulosum and $b*$ (Fig. 8). We did not find any significant correlation between the mean maximum fluorescence intensities corresponding to the τ_2 lifetime and $L*$, $a*$, or $b*$ values (data not shown).

Figure 9 juxtaposes the mean maximum fluorescence intensities corresponding with the τ_1 lifetime in the dorsal and volar skin at each skin layer. The data from the African volunteer's

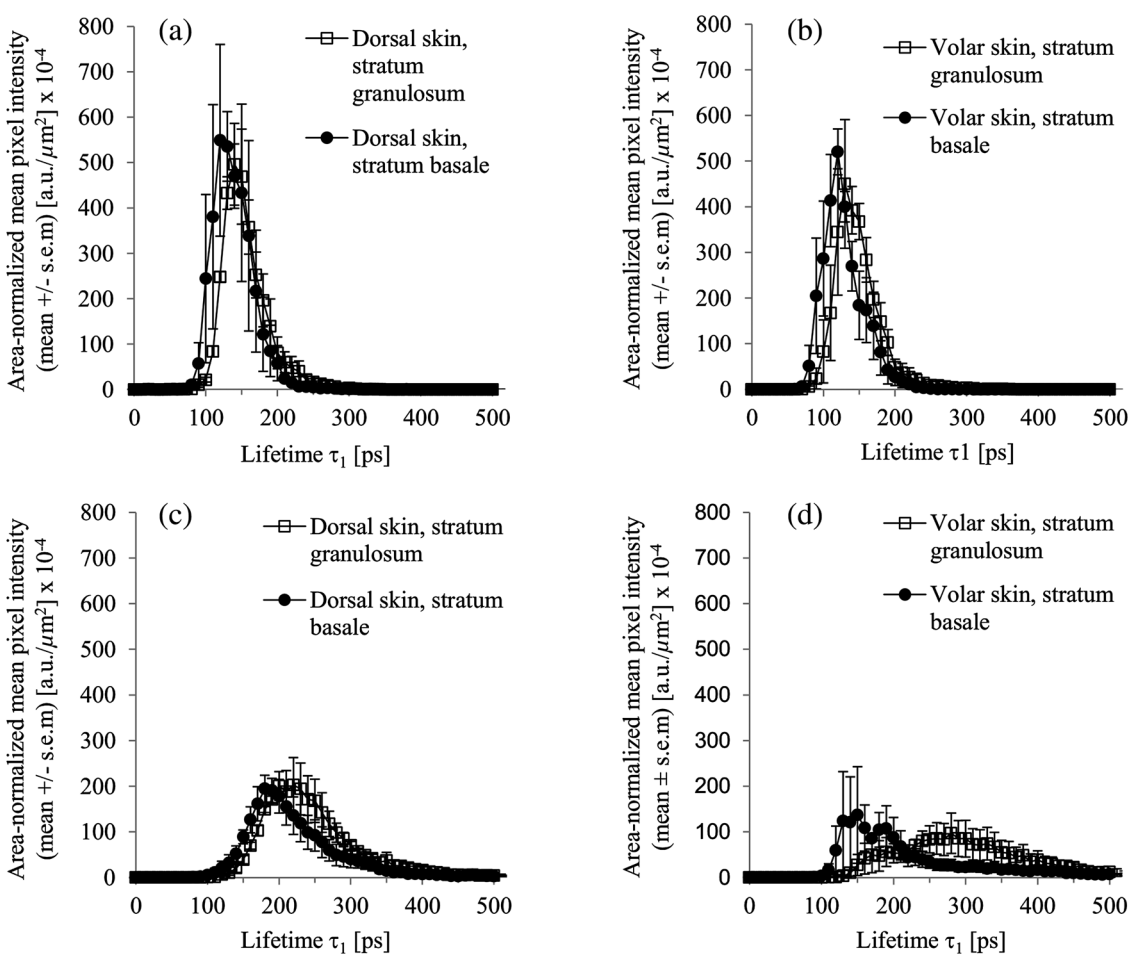

Fig. 5 Area-normalized fluorescence intensity profiles corresponding to the fast (τ_1) lifetime from the dorsal and volar skin of (a) and (b) the African volunteer and (c) and (d) the Asian volunteer.

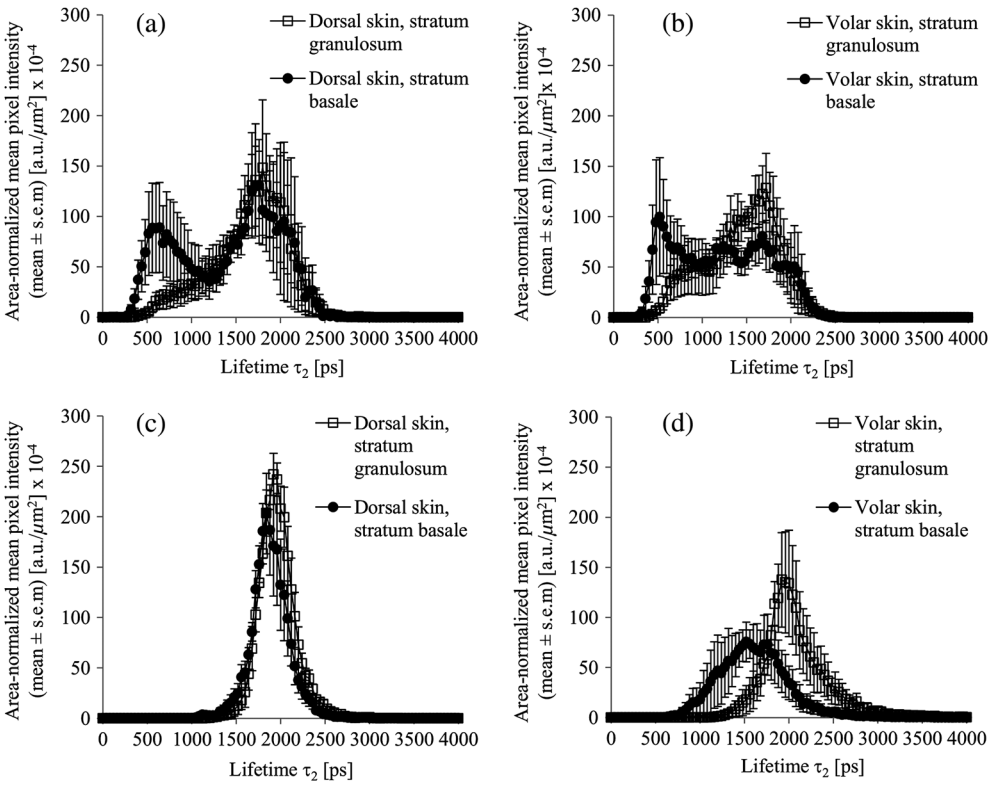

Fig. 6 Area-normalized fluorescence intensity profiles corresponding to the slow (τ_2) lifetime from the dorsal and volar skin of (a) and (b) the African volunteer and (c) and (d) the Asian volunteer.

skin suggest a higher mean fluorescence intensity in the stratum basale than in the stratum granulosum. Such a pattern is not seen in the data from the other skin types, consistent with results in Fig. 7.

4 Discussion

4.1 *Synthetic Melanin Solutions*

Our results with melanin solutions of varying concentrations show that the fluorescence intensity measured from a solution increases linearly with melanin concentration [Fig. 1(b) through 1(f)]. The slopes of the maximum pixel intensity versus melanin concentration curves are in good agreement with that of Gallas et al.'s curve of fluorescence intensity versus melanin for an excitation wavelength of 440 nm (Fig. 3 in Ref. 66), which is close to the equivalent two-photon excitation wavelength we used (800 nm). From this result we inferred that we could expect differences in melanin concentration in skin *in vivo* to be measured based on differences in fluorescence intensity. This is further corroborated by Ait El Madani et al.'s results showing an increase in two-photon excited fluorescence signal intensity with increasing melanin density in human skin.[53]

The τ_1 and τ_2 fluorescence lifetime values we obtained from the synthetic melanin solutions are close to the first two lifetimes reported by Teuchner et al.[54,55] and Nighswander-Rempel et al.[32] for synthetic melanin dissolved in dimethyl sulfoxide (DMSO) and water, respectively (Table 1). Unlike those authors, however, we did not observe a third lifetime component as all the fluorescence decay curves [e.g., Fig. 1(a)] displayed biexponential decay only. One reason for the difference may be Teuchner et al.'s use of stepwise multiphoton excitation rather than simultaneous excitation. The stepwise multiphoton excitation was capable of achieving improved selectivity of melanin excitation, resulting in the greater suppression of background skin autofluorescence and greater melanin imaging contrast.[32,49]

4.2 *Cell Cultures*

By selectively exciting the melanin in melanocytes in a melanocyte-keratinocyte coculture at 800 nm [Fig. 2(a) and 2(b)], we confirmed results by Dimitrow et al.,[24] which show that the melanocytes could be selectively excited on the basis of the laser excitation wavelength. The fluorescence lifetimes and amplitudes we measured in melanocytes [Fig. 3(a) through 3(c)] are in close agreement with values obtained by Dimitrow et al.[24] and Sugata et al.[60] from cell cultures and *in vivo*, respectively (Tables 1 and 2). Figure 2(b) shows that melanin was detected in the melanocytes; no transfer to the keratinocytes occurred. The measured fluorescence is strictly from melanin produced in the melanocytes. There is no evidence to date suggesting that the HaCat keratinocytes contribute to any potential eumelanogenesis within a period of 24 h postseeding and without stimulation.

4.3 *Human Skin In Vivo*

Dimitrow et al. showed images of melanocytes in melanoma skin.[24] We were not able to identify melanocytes in our *in vivo* images. This is likely due to the fact that we imaged healthy skin and that the melanocytes, which occur in a density of 1 melanocyte per 16 to 32 keratinocytes in healthy skin,[67] were not visible at our resolution, making it difficult to distinguish melanocytes from keratinocytes.

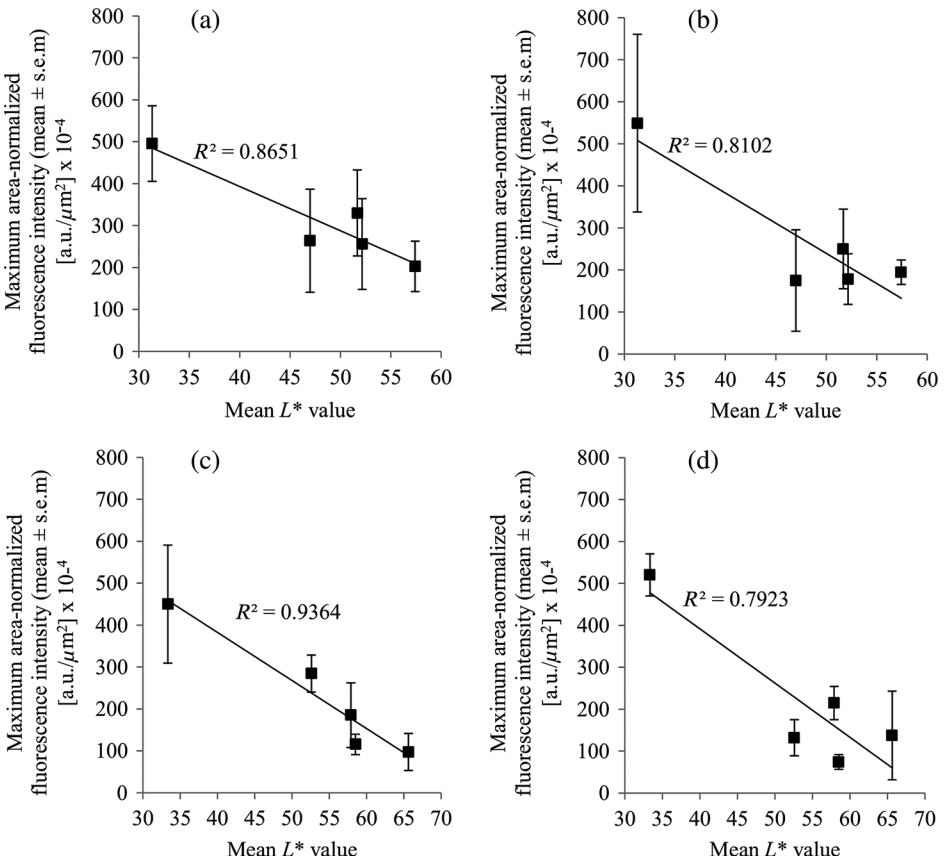

Fig. 7 Maximum area-normalized fluorescence intensity corresponding to the lifetime τ_1 in stratum granulosum and stratum basale versus mean $L*$ value (Table 4) in (a) dorsal stratum granulosum; (b) dorsal stratum basale; (c) volar stratum granulosum; and (d) volar stratum basale. Data (mean ± s.e.m.) from the five volunteers.

The τ_1 lifetimes corresponding to the maximum fluorescence intensities on the dorsal and volar side of the African volunteer's skin ($\tau_1 = 120$ to 140 ps) are in very good agreement with the fast lifetimes attributed primarily to melanin fluorescence in Dimitrow et al.[24] and Sugata et al.'s[60] *in vivo* studies (Table 3). In the Asian volunteer's skin the τ_1 lifetimes corresponding to peak intensities are somewhat higher ($\tau_1 = 150$ to 220 ps) but also agree with published values. The τ_2 lifetimes corresponding with the maximum fluorescence intensities, ranging from $\tau_2 = 1680$ to 1920 ps, are also close to Dimitrow et al. and Sugata et al.'s published slow lifetime values. We obtained additional peaks in the fluorescence intensity at $\tau_2 = 520$ and 640 ps in the stratum basale of the African volunteer's dorsal and volar skin. These values are difficult to interpret. They are close to the τ_2 values obtained by Sugata et al.[60] in a hair bulb (Table 3), but we were not imaging at depths at which the hair bulbs are found. These τ_2 values might indicate that some melanin is packed in melanosomes of African skin in a similar fashion to melanin found in hair. At this stage though, the τ_2 values are not sufficiently informative to draw any conclusions from them.

To measure differences in melanin content in layers of the viable epidermis (stratum granulosum and stratum basale) of a given volunteer and across skin types, we focused on the maximum fluorescence intensity obtained from fluorescence lifetime measurements. The maximum fluorescence intensity associated with the τ_1 lifetimes is the most useful in revealing differences in skin pigmentation. The peak intensities obtained from the dorsal skin of the African volunteer's skin are two to three times greater than from the dorsal skin of the Asian volunteer [Fig. 5(a) versus 5(c)]. The data from the volar sides show four- to fivefold greater peak fluorescence intensities in African versus Asian skin [Fig. 5(b) versus 5(d)]. These results are in agreement with Tadokoro et al.'s data showing the melanin content of unirradiated Black skin being roughly five times greater than unirradiated Asian skin[4] and consistent with other results showing an increase in melanin concentration with pigmentation.[8,11,68]

Whereas there is almost no variation between fluorescence intensities in the dorsal and volar side of the African volunteer's skin [Fig. 5(a) versus 5(b)], in the Asian skin, the mean intensity measured in the stratum granulosum is about two times greater on the dorsal side than the volar side. The mean intensities measured in the stratum basale differ by a factor of 1.4 [Fig. 5(c) versus 5(d)]. Our results from Asian skin agree with Alaluf et al.'s who have measured a total melanin concentration in photoexposed skin of Chinese volunteers that is about 1.5 times greater than in photoprotected skin, with a difference in mean $L*$ values of 10.7 (Ref. 8), comparable to our $\Delta L* = 8.20$ for the Asian volunteer (Table 4). Their results also yielded a 1.8-fold difference in African skin, but their difference in mean $L*$ values is 11, whereas in our study, $\Delta L* = 2.04$ for the African skin (Table 4).

The $L*$ value is the primary tristimulus value, which correlates with total epidermal melanin content.[63] While our method is appropriate for quantifying difference in melanin content between highly pigmented African skin and lightly pigmented Asian skin, it is not sufficiently precise to resolve differences in melanin concentration within the cluster of lighter skin types,

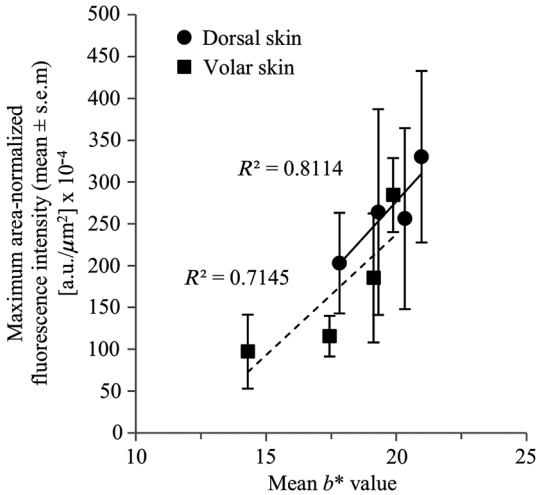

Fig. 8 Maximum area-normalized fluorescence intensity corresponding to the lifetime τ_1 versus mean $b*$ value in dorsal and volar stratum granulosum (Table 4). Data (mean ± s.e.m.) from the five volunteers.

for which $L* \approx 47$ to 66. This is seen in the fact that the correlation seen in Fig. 7(a) through 7(d) are much weaker when the African skin data are removed, and by the lack of a gradient in mean maximum melanin intensity with skin depth comparable to that obtained for African skin (Fig. 9). A likely explanation is the fact that melanosomes in lightly pigmented skin are smaller and mainly distributed in clusters, whereas in African skin they are mainly dispersed as larger, individual particles.[3,8,63] Clusters of melanosomes in lightly pigmented skin may be dispersed less uniformly than individual particles in African skin, yielding inconsistent results when comparing melanin fluorescence intensity and measurements of visible skin color.

Alaluf et al. have also shown a strong exponential correlation between total epidermal content and $a*$ (redness), owing to the fact that melanin reflects large amounts of red incident light.[63] We did not obtain meaningful correlations between $a*$ and the fluorescence intensities associated with τ_1 or τ_2, probably due to our small number of data points. We obtained a positive correlation between the $b*$ value and the maximum fluorescence intensity skin associated with lifetime τ_1 measured in the stratum granulosum, though not the stratum basale, of the lighter pigmented Indian, Caucasian, and Asian volunteers (Fig. 8).

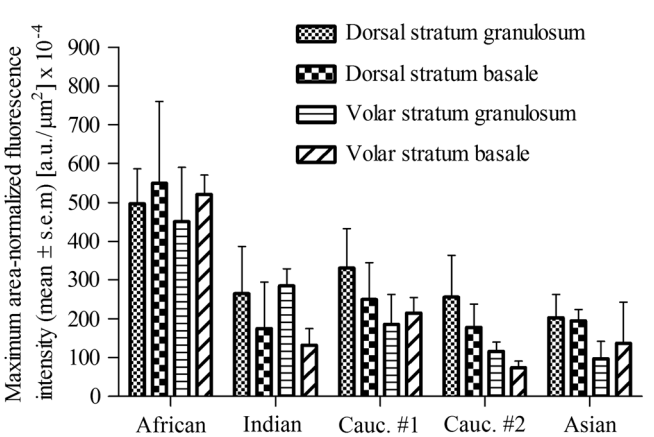

Fig. 9 Maximum area-normalized fluorescence intensity corresponding to the lifetime τ_1 versus skin type. Data (mean ± s.e.m.) from the five volunteers.

This result agrees with Alaluf et al.'s data[63] and further confirms that the fluorescence signal associated with τ_1 reflects melanin.

We did not obtain any meaningful correlation between maximum fluorescence intensities associated with the τ_2 lifetime and $L*$. Making sense of the peak fluorescence intensities corresponding with τ_2 lifetimes is difficult. Peak fluorescence intensities obtained from the volar skin overlap, whereas values from the dorsal side corresponding with $\tau_2 = 1760$ to 1920 ps are about 1.6 times higher in Asian skin than in African skin. A correlation between maximum fluorescence intensity and skin pigmentation was not obtained. While the lifetime τ_1 is a signature of melanin fluorescence, the fluorescence associated with lifetime τ_2 may reflect the interaction of melanin with protein in the cellular environment such as nicotinamide adenine dinucleotide phosphate (NAD(P)H), as its two-photon excitation wavelength overlaps with that of melanin and its range of emission wavelengths is close.[13] This would explain the nearly overlapping fluorescence intensity profiles associated with τ_2 measured African and Asian skin. Due to the protein in our synthetic melanin solution, similar correlations were found between maximum fluorescence intensity and lifetimes τ_1 and τ_2 [Fig. 1(e) and 1(f)].

In general, a certain percentage of the fluorescence we observed in the skin of volunteers is likely also due to other skin fluorophores such as NADH and FAD. The contribution of NADH is assumed minimal due to its maximum emission wavelength around 450 nm (Refs. 69 and 70) being outside of the range of detected emission used in this study (515 to 620 nm). FAD, however, may be a more significant confounder. The FAD maximum emission wavelength overlaps with that of melanin at about 525 nm (Refs. 69 and 71). The quantum yield of neutral FAD has been reported as 0.03 (Ref. 5), whereas that of synthetic eumelanin is on the order of 10^{-4} (Ref. 4).

One may be able to improve detection efficiency of melanin fluorescence, in particular as a function of depth into the skin (Fig. 9), by using optical clearing agents. Glycerol and DMSO in solution have been shown to reduce skin optical scattering and increase optical penetration depth.[38,72] However, issues of systemic toxicity of DMSO must be resolved prior to use with volunteers.[72] We may also achieve enhanced detection of melanin by using stepwise instead of simultaneous two-photon absorption. Eichhorn et al. have shown stepwise multiphoton excitation to be effective in selectively exciting melanin and suppressing FAD excitation.[71] Furthermore, Kerimo et al. have shown that Sepia melanin was efficiently excited by three-photon excitation.[73]

Finally, a larger study with more than one African, Indian, and Asian volunteer is needed in order to show that the differences in maximum fluorescence intensities (Fig. 9) are statistically significant.

5 Conclusion

We have shown that MPT and FLIM can be used to noninvasively measure differences in melanin concentration in skin *in vivo* when comparing darkly pigmented and lightly pigmented skin types (African versus Asian) and at different depths within African skin. Further improvements in the technique are required in order to resolve differences in melanin concentration and distribution in skin types of similar reflectance ($L*$ values). A detailed understanding of relationships linking melanin concentration and distribution and visible skin color is of primary importance in studies of pigmentation-related diseases, the continued development of MPT and FLIM as noninvasive

diagnostic tools for such diseases, and the design of drugs and cosmetic products targeting cutaneous melanin.

Acknowledgments

We thank the Australian Research Council (ARC) and Johnson & Johnson for an ARC Linkage Grant. M.R. was supported by the Australian National Health & Medical Research Council. Y.D. acknowledges Dr. Andrew J. Dalley for invaluable help with cell cultures and Dr. Nikiforos Kollias, Dr. Tarl Prow, and Dr. Peter Soyer for fruitful discussions.

References

1. R. Gunathilake et al., "pH-regulated mechanisms account for pigment-type differences in epidermal barrier function," *J. Invest. Dermatol.* **129**(7), 1719–1729 (2009).
2. P. M. Elias et al., "Evidence that stress to the epidermal barrier influenced the development of pigmentation in humans," *Pigm. Cell Melanoma Res.* **22**(4), 420–434 (2009).
3. H. Y. Thong et al., "The patterns of melanosome distribution in keratinocytes of human skin as one determining factor of skin colour," *The British J. Dermatol.* **149**(3), 498–505 (2003).
4. T. Tadokoro et al., "Mechanisms of skin tanning in different racial/ethnic groups in response to ultraviolet radiation," *J. Invest. Dermatol.* **124**(6), 1326–1332 (2005).
5. Y. Yamaguchi et al., "Human skin responses to UV radiation: pigment in the upper epidermis protects against DNA damage in the lower epidermis and facilitates apoptosis," *FASEB J.* **20**(9), 1486–1488 (2006).
6. J. D. Bancroft and A. Stevens, *Theory and Practice of Histological Techniques*, Churchill Livingstone, New York (1982).
7. L. Minwalla et al., "Keratinocytes play a role in regulating distribution patterns of recipient melanosomes in vitro," *J. Invest. Dermatol.* **117**(2), 341–347 (2001).
8. S. Alaluf et al., "Ethnic variation in melanin content and composition in photoexposed and photoprotected human skin," *Pigm. Cell Res.* **15**(2), 112–118 (2002).
9. J. A. Viator et al., "A comparative study of photoacoustic and reflectance methods for determination of epidermal melanin content," *J. Invest. Dermatol.* **122**(6), 1432–1439 (2004).
10. F. Helmchen and W. Denk, "Deep tissue two-photon microscopy," *Nat. Methods* **2**(12), 932–940 (2005).
11. W. R. Zipfel, R. M. Williams, and W. W. Webb, "Nonlinear magic: multiphoton microscopy in the biosciences," *Nature Biotech.* **21**(11), 1369–1377 (2003).
12. B. G. Wang, K. Konig, and K. J. Halbhuber, "Two-photon microscopy of deep intravital tissues and its merits in clinical research," *J. Microsc.* **238**(1), 1–20 (2010).
13. M. S. Roberts et al., "Non-invasive imaging of skin physiology and percutaneous penetration using fluorescence spectral and lifetime imaging with multiphoton and confocal microscopy," *Eur. J. Pharm. Biopharm.* **77**(3), 469–488 (2011).
14. D. Chorvat, Jr. and A. Chorvatova, "Multi-wavelength fluorescence lifetime spectroscopy: a new approach to the study of endogenous fluorescence in living cells and tissues," *Laser. Phys. Lett.* **6**(3), 175–193 (2009).
15. W. Becker, "Fluorescence lifetime imaging—techniques and applications," *J. Microsc.* **247**(2), 119–136 (2012).
16. K. Konig and I. Riemann, "High-resolution multiphoton tomography of human skin with subcellular spatial resolution and picosecond time resolution," *J. Biomed. Opt.* **8**(3), 432–439 (2003).
17. L. H. Laiho et al., "Two-photon 3-D mapping of *ex vivo* human skin endogenous fluorescence species based on fluorescence emission spectra," *J. Biomed. Opt.* **10**(2), 024016 (2005).
18. J. A. Palero et al., "Spectrally resolved multiphoton imaging of *in vivo* and excised mouse skin tissues," *Biophys. J.* **93**(3), 992–1007 (2007).
19. W. Y. Sanchez et al., "Analysis of the metabolic deterioration of *ex vivo* skin from ischemic necrosis through the imaging of intracellular NAD(P)H by multiphoton tomography and fluorescence lifetime imaging microscopy," *J. Biomed. Opt.* **15**(4), 046008 (2010).
20. M. S. Roberts et al., "*In vitro* and *in vivo* imaging of xenobiotic transport in human skin and in the rat liver," *J. Biophotonics* **1**(6), 478–493 (2008).
21. C. A. Thorling et al., "Multiphoton microscopy and fluorescence lifetime imaging provide a novel method in studying drug distribution and metabolism in the rat liver *in vivo*," *J. Biomed. Opt.* **16**(8), 086013 (2011).
22. K. Konig et al., "*In vivo* multiphoton tomography of skin cancer," *Proc. SPIE* **6089**, 60890R (2006).
23. J. Paoli et al., "Multiphoton laser scanning microscopy on non-melanoma skin cancer: morphologic features for future non-invasive diagnostics," *J. Invest. Dermatol.* **128**(5), 1248–1255 (2007).
24. E. Dimitrow et al., "Spectral fluorescence lifetime detection and selective melanin imaging by multiphoton laser tomography for melanoma diagnosis," *Exp. Dermatol.* **18**(6), 509–515 (2009).
25. E. Dimitrow et al., "Sensitivity and specificity of multiphoton laser tomography for *in vivo* and *ex vivo* diagnosis of malignant melanoma," *J. Invest. Dermatol.* **129**(7), 1752–1758 (2009).
26. P. P. Provenzano, K. W. Eliceiri, and P. J. Keely, "Multiphoton microscopy and fluorescence lifetime imaging microscopy (FLIM) to monitor metastasis and the tumor microenvironment," *Clin. Exp. Metastasis* **26**(4), 357–370 (2009).
27. M. J. Koehler et al., "Clinical application of multiphoton tomography in combination with confocal laser scanning microscopy for *in vivo* evaluation of skin diseases," *Exp. Dermatol.* **20**(7), 589–594 (2011).
28. P. B. Jones et al., "Two postprocessing techniques for the elimination of background autofluorescence for fluorescence lifetime imaging microscopy," *J. Biomed. Opt.* **13**(1), 014008 (2008).
29. K. Konig et al., "Clinical application of multiphoton tomography in combination with high-frequency ultrasound for evaluation of skin diseases," *J. Biophoton.* **3**(12), 759–773 (2010).
30. K. Dowling et al., "Fluorescence lifetime imaging with picosecond resolution for biomedical applications," *Opt. Lett.* **23**(10), 810–812 (1998).
31. A. Zoumi, A. Yeh, and B. J. Tromberg, "Imaging cells and extracellular matrix *in vivo* by using second-harmonic generation and two-photon excited fluorescence," *Proc. Natl. Acad. Sci. U. S. A.* **99**(17), 11014–11019 (2002).
32. R. Eichhorn et al., "Early diagnosis of melanotic melanoma based on laser-induced melanin fluorescence," *J. Biomed. Opt.* **14**(3), 034033 (2009).
33. N. Nakashima et al., "Picosecond fluorescence lifetime of the coenzyme of D-amino acid oxidase," *J. Biol. Chem.* **255**(11), 5261–5263 (1980).
34. P. A. De Beule et al., "A hyperspectral fluorescence lifetime probe for skin cancer diagnosis," *Review Sci. Instr.* **78**(12), 123101 (2007).
35. A. Pena et al., "Spectroscopic analysis of keratin endogenous signal for skin multiphoton microscopy," *Opt. Express* **13**(16), 6268–6274 (2005).
36. A. Ehlers et al., "Multiphoton fluorescence lifetime imaging of human hair," *Microsc. Res. Tech.* **70**(2), 154–161 (2007).
37. E. R. Gaillard et al., "Photophysical studies on human retinal lipofuscin," *Photochem. Photobio.* **61**(5), 448–453 (1995).
38. R. Cicchi et al., "Contrast and depth enhancement in two-photon microscopy of human skin *ex vivo* by use of optical clearing agents," *Opt. Express* **13**(7), 2337–2344 (2005).
39. B. R. Masters, P. T. So, and E. Gratton, "Multiphoton excitation fluorescence microscopy and spectroscopy of *in vivo* human skin," *Biophys. J.* **72**(6), 2405–2412 (1997).
40. M. C. Skala et al., "*In vivo* multiphoton fluorescence lifetime imaging of protein-bound and free nicotinamide adenine dinucleotide in normal and precancerous epithelia," *J. Biomed. Opt.* **12**(2), 024014 (2007).
41. V. V. Ghukasyan and F.-J. Kao, "Monitoring cellular metabolism with fluorescence lifetime of reduced nicotinamide adenine dinucleotide," *J. Phys. Chem. C* **113**(27), 11532–11540 (2009).
42. H. Schneckenburger et al., "Time-resolved *in-vivo* fluorescence of photosensitizing porphyrins," *J. Photochem. Photobiol. B Biol.* **21**(2–3), 143–147 (1993).
43. R. Cubeddu et al., "Fluorescence lifetime imaging: an application to the detection of skin tumors," *IEEE J. Sel. Top. Quantum Electron.* **5**(4), 923–929 (1999).
44. K. Konig, "Multiphoton microscopy in life sciences," *J. Microsc.* **200**(2), 83–104 (2000).

45. M. Collini et al., "Probing protein aggregation by time-resolved fluorescence during beta-lactoglobulin crystal growth," *Eur. Biophys. J.* **31**(2), 111–117 (2002).
46. W. R. Zipfel et al., "Live tissue intrinsic emission microscopy using multiphoton-excited native fluorescence and second harmonic generation," *Proc. Natl. Acad. Sci. U. S. A.* **100**(12), 7075–7080 (2003).
47. Q. Wang, J. C. Allen, and H. E. Swaisgood, "Binding of vitamin D and cholesterol to beta-lactoglobulin," *J. Dairy Sci.* **80**(6), 1054–1059 (1997).
48. E. Brown et al., "Dynamic imaging of collagen and its modulation in tumors *in vivo* using second-harmonic generation," *Nat. Med.* **9**(6), 796–800 (2003).
49. D. Leupold et al., "The stepwise two-photon excited melanin fluorescence is a unique diagnostic tool for the detection of malignant transformation in melanocytes," *Pigm. Cell Melanoma Res.* **24**(3), 438–445 (2011).
50. C. B. Talbot et al., "Application of ultrafast gold luminescence to measuring the instrument response function for multispectral multiphoton fluorescence lifetime imaging," *Opt. Express* **19**(15), 13848–13861 (2011).
51. T. Ye et al., "Imaging melanin by two-photon absorption microscopy," *Proc. SPIE* **6089**, 60891X (2006).
52. C. Antoniou et al., "Analysis of the melanin distribution in different ethnic groups by *in vivo* laser scanning miscroscopy," *Laser Phys. Lett.* **6**(5), 393–398 (2009).
53. S. W. Perry, R. M. Burke, and E. B. Brown, "Two-photon and second harmonic microscopy in clinical and translational cancer research," *Ann. Bio. Eng.* **40**(2), 277–291 (2012).
54. K. Teuchner et al., "Fluorescence studies of melanin by stepwise two-photon femtosecond laser excitation," *J. Fluoresc.* **10**(3), 275–281 (2000).
55. S. Wang et al., "Monte Carlo simulation of near infrared autofluorescence measurements of *in vivo* skin," *J. Photochem. Photobiol. B Biol.* **105**(3), 183–189 (2011).
56. S. E. Forest et al., "A model for the activated energy transfer within eumelanin aggregates," *J. Physical Chem. B* **104**(4), 811–814 (2000).
57. T. Gambichler et al., "Effects of repeated sunbed exposures on the human skin. *In vivo* measurements with confocal microscopy," *Photodermatol. Photoimmunol. Photomed.* **20**(1), 27–32 (2004).
58. E. Benati et al., "Quantitative evaluation of healthy epidermis by means of multiphoton microscopy and fluorescence lifetime imaging microscopy," *Skin Res. Technol.* **17**(3), 295–303 (2011).
59. D. Fu et al., "Two-color, two-photon, and excited-state absorption microscopy," *J. Biomed. Opt.* **12**(5), 054004 (2007).
60. K. Sugata et al., "Imaging of melanin distribution using multiphoton autofluorescence decay curves," *Skin Res. Technol.* **16**(1), 55–59 (2010).
61. M. Kaatz et al., "Depth-resolved measurement of the dermal matrix composition by multiphoton laser tomography," *Skin Res. Technol.* **16**(2), 131–136 (2010).
62. M. J. Koehler et al., "Morphological skin ageing criteria by multiphoton laser scanning tomography: non-invasive *in vivo* scoring of the dermal fibre network," *Exp. Dermatol.* **17**(6), 519–523 (2008).
63. S. Alaluf et al., "The impact of epidermal melanin on objective measurements of human skin colour," *Pigm. Cell Res.* **15**(2), 119–126 (2002).
64. K. König et al., "Optical skin biopsies by clinical CARS and multiphoton fluorescence/SHG tomography," *Laser Phys. Lett.* **8**(6), 465–468 (2011).
65. W. Becker, "Fluorescence lifetime imaging–techniques and applications," *J. Microsc.* **247**(2), 119–136 (2012).
66. D. Chorvat, Jr. et al., "Rejection of transplanted hearts in patients evaluated by the component analysis of multi-wavelength NAD(P)H fluorescence lifetime spectroscopy," *J. Biophoton.* **3**(10–11), 646–652 (2010).
67. X. Jiang et al., "Multiphoton microscopic imaging of *in vivo* hair mouse skin based on two-photon excited fluorescence and second harmonic generation," *Scanning* **34**(3), 170–173 (2012).
68. K. Konig et al., "Applications of multiphoton tomographs and femtosecond laser nanoprocessing microscopes in drug delivery research," *Adv. Drug Deliv. Rev.* **63**(4–5), 388–404 (2011).
69. S. H. Huang, A. A. Heikal, and W. W. Webb, "Two-photon fluorescence spectroscopy and microscopy of NAD(P)H and flavoprotein," *Biophys. J.* **82**(5), 2811–2825 (2002).
70. W. R. Zipfel et al., "Live tissue intrinsic emission microscopy using multiphoton-excited native fluorescence and second harmonic generation," *Proc. Natl. Acad. Sci. U. S. A.* **100**(12), 7075–7080 (2003).
71. R. Eichhorn et al., "Early diagnosis of melanotic melanoma based on laser-induced melanin fluorescence," *J. Biomed. Opt.* **14**(3), 034033 (2009).
72. A. K. Bui et al., "Revisiting optical clearing with dimethyl sulfoxide (DMSO)," *Lasers Surg. Med.* **41**(2), 142–148 (2009).
73. J. Kerimo, M. Rajadhyaksha, and C. A. DiMarzio, "Enhanced melanin fluorescence by stepwise three-photon excitation," *Photochem. Photobiol.* **87**(5), 1042–1049 (2011).